RZ 3899 (#ZUR1501-006) 01/06/2015
Physical Sciences 11 pages

Research Report

On-surface generation and imaging of arynes by atomic force microscopy

Niko Pavliček,[1] Bruno Schuler,[1] Sara Collazos,[2] Nikolaj Moll,[1] Dolores Pérez,[2] Enrique Guitián,[2] Gerhard Meyer,[1] Diego Peña,[2] and Leo Gross[1]

[1]IBM Research – Zurich, 8803 Rüschlikon, Switzerland

[2]CIQUS, Universidad de Santiago de Compostela, 15782 Santiago de Compostela, Spain

This is the author's version of the work. The definitive version was published in *Nature Chemistry*, vol. 7, no. 8, pp. 623–628 (2015) (doi:10.1038/nchem.2300; published online 13 July 2015) and can be accessed here:
http://www.nature.com/nchem/journal/v7/n8/abs/nchem.2300.html

On-surface generation and imaging of arynes by atomic force microscopy

Niko Pavliček[1]*, Bruno Schuler[1], Sara Collazos[2], Nikolaj Moll[1], Dolores Pérez[2], Enrique Guitián[2], Gerhard Meyer[1], Diego Peña[2]† and Leo Gross[1]

1. IBM Research–Zurich, 8803 Rüschlikon, Switzerland
2. CIQUS, Universidad de Santiago de Compostela, 15782 Santiago de Compostela, Spain

22nd May 2015

Reactive intermediates are involved in most chemical transformations. However, their characterization is a great challenge because of their short lifetime and high reactivity. Arynes are prominent reactive intermediates, formally derived from arenes by removal of two hydrogen atoms from adjacent carbon atoms. Their rich chemistry enables widespread use in synthetic chemistry, as they are privileged building blocks for the construction of polycyclic compounds containing aromatic rings. Here, we demonstrate generation and characterization of individual polycyclic aryne molecules on an ultra-thin insulating film by means of low-temperature scanning tunnelling and atomic force microscopy. In addition, our results provide important insights into the chemistry of these elusive intermediates and its potential application in the field of on-surface synthesis.

Introduction

The history of the short-lived aryne species dates back to 1902[1,2], although conclusive experimental evidence of the intermediacy of benzyne—C_6H_4, the parent member of the aryne family—in a chemical transformation was reported only in the 50's by Roberts[3]. Far from being mere chemical curiosities, arynes soon proved to be useful synthetic tools as suitable methods for their generation in diverse reaction environments became available[4]. When generated in the presence of adequate reaction partners, they undergo a variety of chemical transformations, which enable a plethora of applications in synthesis[5–8]. Recent examples include the construction of very large polycyclic aromatic hydrocarbons[9,10], the use of pyridynes as building blocks[11], or the chemical modification of graphene sheets[12] and carbon nanotubes[13]. Moreover, recent approaches to generate benzynes by cycloisomerization of triyne precursors have opened unexpected opportunities in aryne chemistry[14–17]. Despite this broad range of practical applications, their structural characterization has been the subject of debate and remains a challenge. Microwave[18] and IR[19] spectroscopic studies on benzyne—and several substituted and annulated derivatives—either in the gas phase or isolated in cryogenic matrices, support an electronic structure best described by a resonant form with a triple bond between two adjacent carbon atoms. However, the solution ^{1}H and ^{13}C NMR spectra of benzyne, generated inside a hemicarcerand molecular container, are in agreement with a cumulene structure[20], whereas theoretical calculations suggest a structure of more acetylenic than cumulenic character[21].

The ability to image and manipulate molecules on the atomic scale makes scanning tunnelling microscopy (STM) a well-suited tool to study on-surface chemistry on the molecular scale[22–24]. Naturally, the ability of atomic force microscopy (AFM) to resolve chemical structures using functionalised tips[25] was an additional boost in this direction[26–29].

*pav@zurich.ibm.com
†diego.pena@usc.es

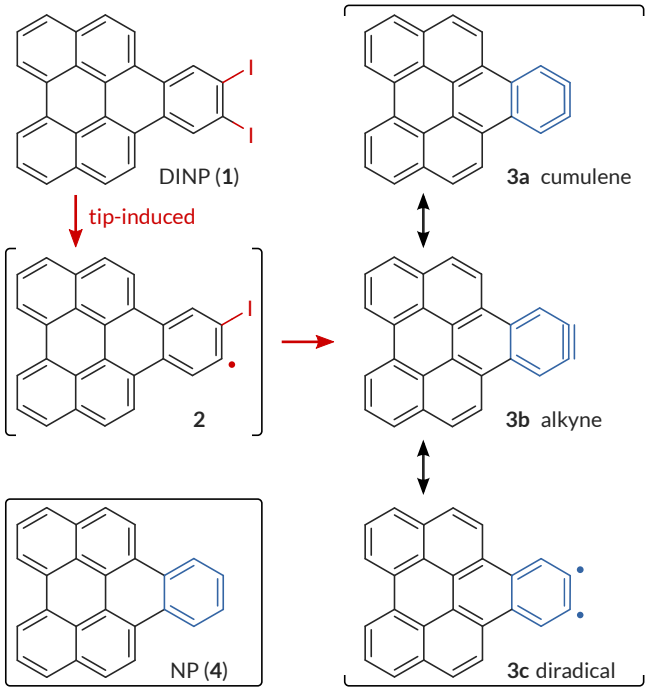

Figure 1: Chemical transformation studied on surface. Starting from DINP (**1**), iodine dissociation generates aryne **3**. Dehalogenation may either occur directly from **1** to **3** or sequentially via intermediate **2**. **3a-c** are the three possible resonance structures of this aryne. NP (**4**) is the fully hydrogenated analogue of aryne **3** and investigated for comparison.

Results and discussion

In this article, we present a novel on-surface method to generate individual aryne molecules on bilayer (100)-terminated films of NaCl on Cu(111) single crystals (denoted as NaCl(2ML)/Cu(111)). Our method is based on dehalogenation[30–32] of an *ortho*-diiodoarene as a precursor using the tip of a combined STM/AFM. High-resolution non-contact AFM is used to directly image the chemical structure of arynes for the first time. Details of the molecular structure are revealed[25,33] by comparison of high resolution AFM measurements of the arynes with that of related compounds. A bond-order analysis[34] suggests that cumulene is the predominant resonance structure in this particular case.

We found that an ultra-thin insulating film as substrate is a prerequisite to stabilize this aryne. Tip-induced dehalogenation of precursor molecules on NaCl(2ML)/Cu(111) produces stable arynes, whereas the same procedure applied to precursors adsorbed directly on Cu(111) results in strong chemical bonding to the underlying metal substrate. As control experiment, we compare images of arynes with their hydrogenated counterparts, unambiguously proving successful generation of stable arynes. In solution chemistry, arynes are generated and trapped *in situ* by adequate reaction partners to form a final product. In strong contrast, the use of low temperatures in combination with an insulating surface creates stable arynes while preserving their high reactivity.

Figure 1 presents the molecular structures involved in the generation process. The starting material is 10,11-diiodonaphtho[1,2,3,4-*ghi*]perylene (DINP, **1**), a molecule with two iodine atoms at the outer benzene ring. Tip-induced iodine dissociation may occur either in a two-step process via radical **2** or directly. The final product after dehalogenation, 10,11-didehydronaphtho[1,2,3,4-*ghi*]perylene (or naphthoperyl*yne*, and simply denoted as aryne below), can be depicted using three resonance structures (**3a-c**). We have deliberately chosen large polycyclic DINP molecules to render bond-order analysis possible[34]. In addition, structure **4** depicts naphtho[1,2,3,4-*ghi*]perylene (NP), which is the pure aromatic hydrocarbon.

STM imaging of DINP and co-adsorbed NP molecules on NaCl(2ML)/Cu(111) is presented in Fig. 2. DINP and NP molecules can be clearly distinguished in the STM topograph shown in Fig. 2a. Voltage-dependent imaging of a single DINP molecule is presented in Figs. 2b-d. We find that only the negative ion resonance, related to the LUMO, (Figs. 2c,d) is in the accessible voltage range. To generate arynes we use a simple vertical manipulation protocol. After initial imaging of DINP molecules, the tip is positioned above the iodine-related end of the molecules (dark red lobes in Fig. 2a). Then, the feedback loop is turned

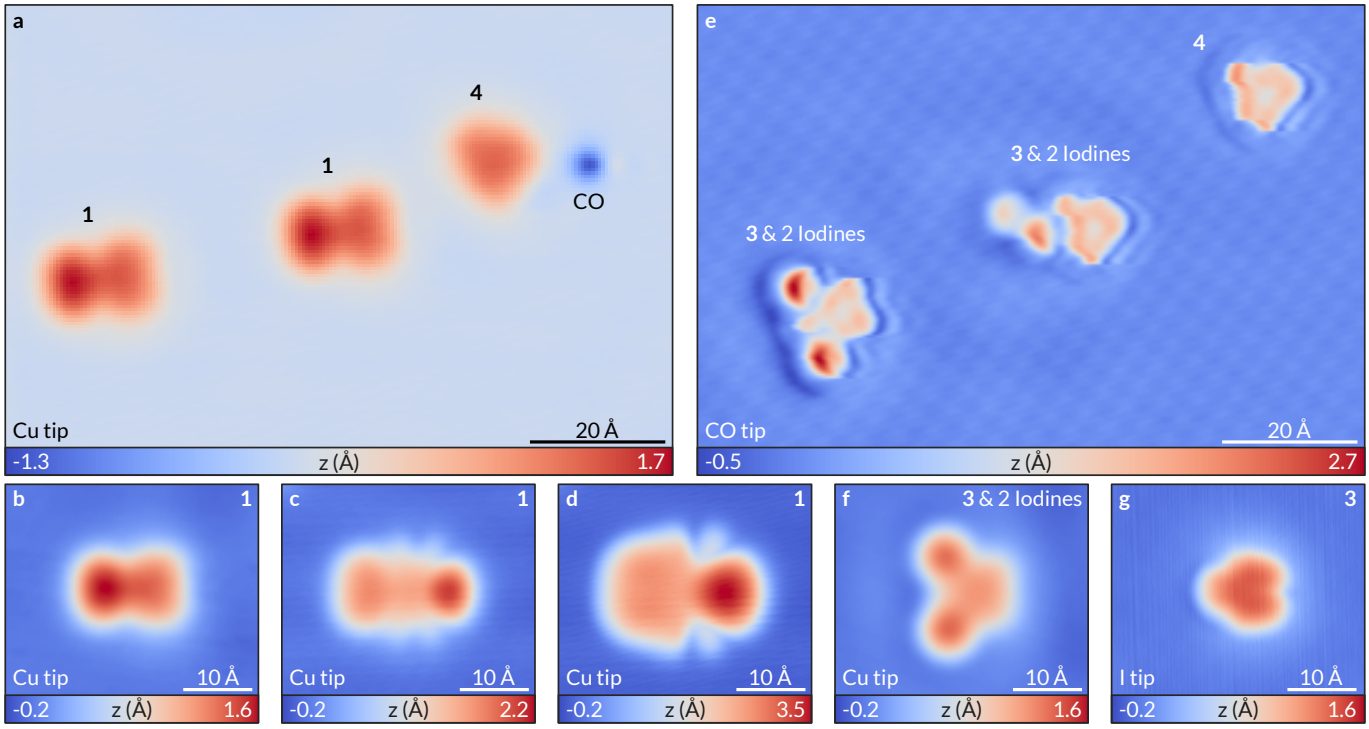

Figure 2: STM imaging and on-surface generation of arynes on NaCl(2ML)/Cu(111). a,e, STM overview images before (acquired with a Cu tip; sample voltage $V = 0.2\,\mathrm{V}$, tunnelling current $I = 2\,\mathrm{pA}$) and after (CO tip; $V = 0.15\,\mathrm{V}$, $I = 2\,\mathrm{pA}$) aryne generation from two DINP molecules (denoted with **1**) on the left-hand side, respectively. Tip-induced dehalogenation is confirmed by the detached iodine atoms lying close-by. **b-d,** Voltage-dependent imaging of a DINP molecule at 0.2 V, 1.6 V (onset of LUMO), and 1.7 V (LUMO), respectively (Cu tip; $I = 2\,\mathrm{pA}$). **f,g,** Zoom-ins on aryne molecules with detached iodine atoms lying nearby (**f**, Cu tip; $V = 0.2\,\mathrm{V}$, $I = 2\,\mathrm{pA}$) and without iodine atoms lying nearby (**g**, I tip; $V = 0.06\,\mathrm{V}$, $I = 5\,\mathrm{pA}$), respectively.

off and the voltage is increased to $V \approx 1.8\,\mathrm{V}$. A sudden change of the tunnelling current, typically within a few seconds, signals successful manipulation. The atomically resolved STM image in Fig. 2e, acquired with a CO-terminated tip (CO tip[25,30]), reveals that the I atoms are now lying next to the molecules. In general, both the molecule and the I atoms are found laterally displaced after manipulation (an additional manipulation sequence is presented in Supplementary Fig. S2). The I atoms could be found several surface lattice constants away from the remainder molecule. Often one I atom and in rare cases both of them (as in Fig. 2e) are found on nearest adsorption sites next to the remainder molecule. Figure 2f, acquired with a Cu-terminated (Cu tip), presents a zoom-in on the left molecule from Fig. 2e: The appearance has changed drastically as compared to that of the initial DINP molecule. After picking up one of the I atoms, recovering a Cu tip, and finally picking up the remaining I atom (leading to an I-terminated tip [I tip]), Fig. 2g presumably represents an STM image of aryne (**3**). We prove below that this is indeed the case.

From our experiments we see that dehalogenation only occurs for voltages $V \gtrsim 1.6\,\mathrm{V}$. This threshold corresponds to resonant tunnelling, suggesting that energy from vibronic excitations[35] is dissipated to cleave the C-I bonds.

In a next step, we have investigated the chemical structure of the compounds involved in the on-surface generation by means of constant-height AFM imaging. In AFM images of DINP molecules (see Figs. 3a and 3f), the bonded I atoms show up as bright, elongated features corresponding to strong repulsive force contributions. As discussed above, I atoms are occasionally found symmetrically on each side of the molecule after dissociation. Figures 3b and 3c present STM images taken directly after such a dissociation event and after picking up one of the I atoms, respectively. The appearance of these individual I atoms strongly differs from that of the bonded ones both in STM and AFM imaging. In corresponding AFM images, shown in Figs. 3d and 3e, the presence of the I atoms leads to apparent distortions of the molecular structure. This effect is explained by strong attractive force contributions between the I atoms and the CO tip. The faint ridges from the iodine and the molecular backbone are reminiscent of intermolecular features, which have been discussed extensively in recent literature[27,36,37], and caused by a ridge naturally arising between two extrema

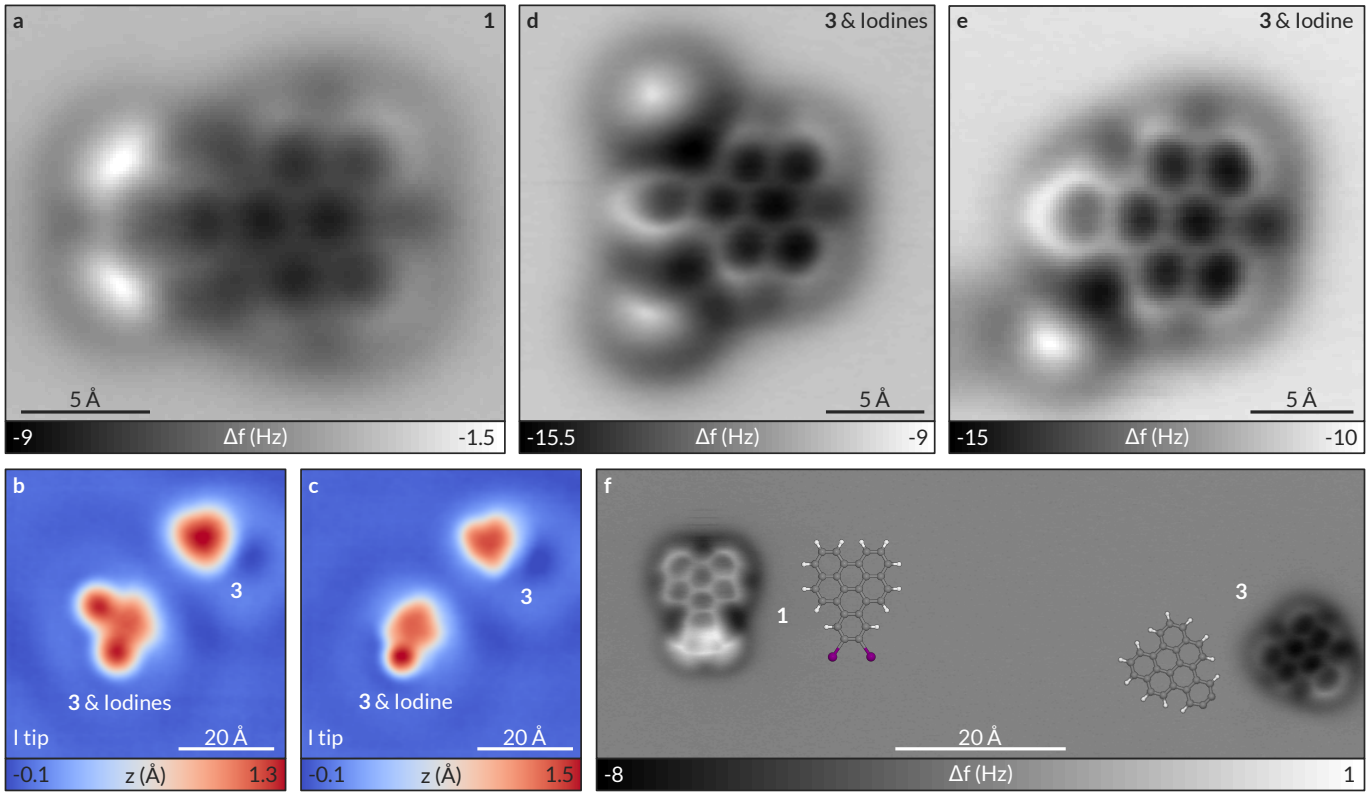

Figure 3: High-resolution AFM imaging of reaction compounds. **a,** AFM image of DINP (**1**) ($\Delta z = -1.1$ Å). **b,c,** Subsequent STM overview images ($V = 0.2$ V, $I = 2$ pA) after iodine dissociation acquired with I tips before (**b**) and after (**c**) picking up one of the I atoms close to the left molecule, respectively. A Cu tip had been recovered before picking up the I atom. **d,e,** Corresponding AFM images of an aryne molecule close to two and one iodine atom, respectively ($\Delta z = -1.2$ Å). **f,** Direct comparison of an DINP (**1**) and an aryne molecule (**3**) in the same frame ($\Delta z = -1.1$ Å); the structures depicted next to the imaged molecules are a guide to the eye.

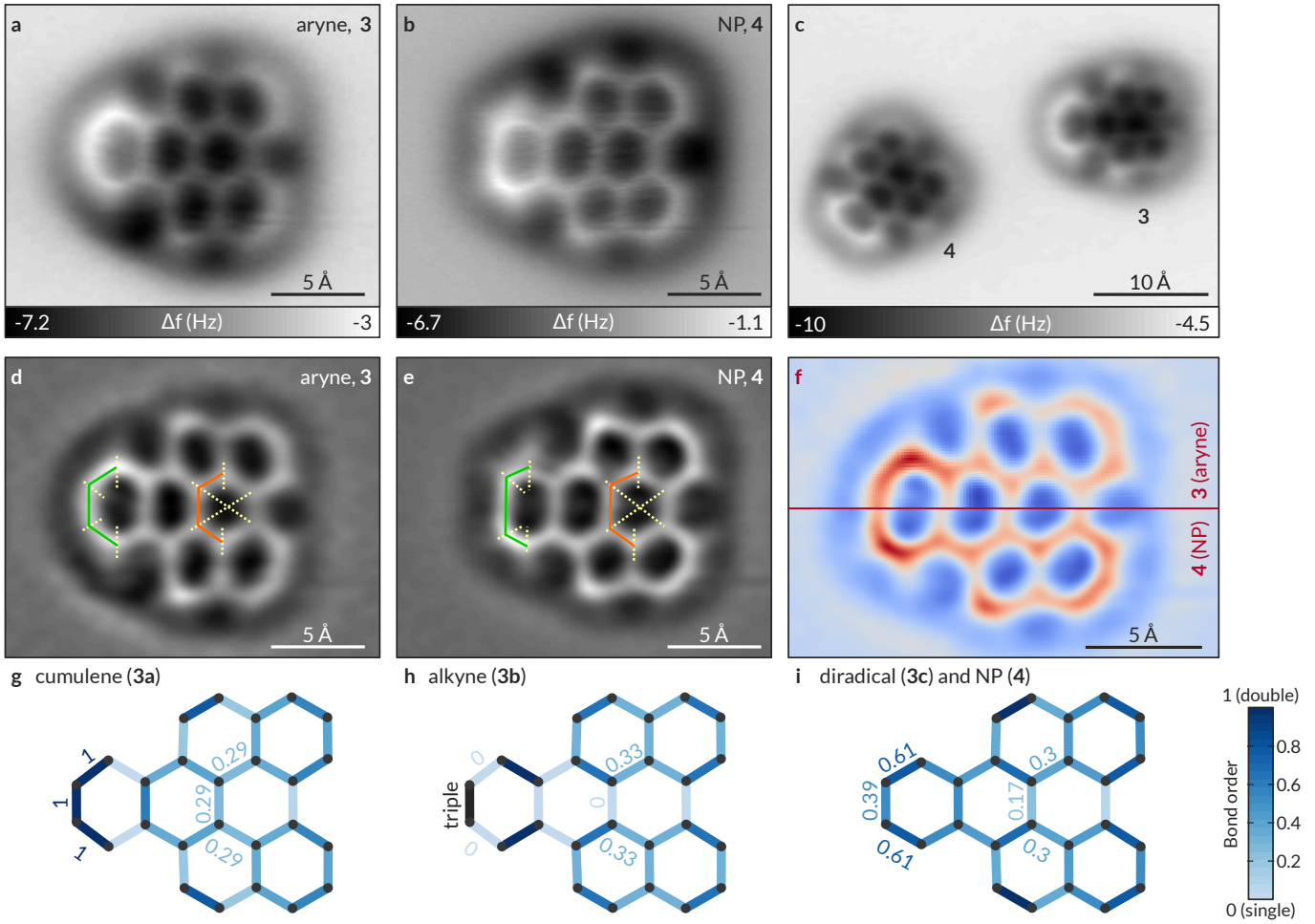

Figure 4: Structure and bond-length evaluation of aryne and NP molecules. a,b, AFM imaging of individual aryne (**3**, $\Delta z = -1.1$ Å) and NP molecules (**4**, $\Delta z = -0.78$ Å), respectively. **c,** AFM image of an aryne (**3**) and an NP molecule (**4**) close to each other ($\Delta z = -1.0$ Å). **d,e,** The Laplace-filtered representations of panels **a** and **b** emphasize their differences. Solid and dashed lines are drawn to highlight differences in the apparent bond lengths. **f**, To facilitate direct comparison, clipped and zoomed-in data from **d** and **e** are shown in the top (aryne **3**) and bottom (NP **4**) part, respectively. The rightmost bond on the symmetry axis was used to align both images. **g-i,** Colour-coded carbon-carbon bond orders for Kekulé depictions **3a**, **3b** or **3c**, respectively. Note that **i** is also valid for NP molecules (**4**).

in the potential energy landscape[34,38,39]. These ridges do not indicate bonds, and similar features have been observed between a Au adatom and a 3,4,9,10-perylenetetracarboxylic dianhydride (PTCDA) molecule without the presence of a bond between them[26]. More importantly, we do not observe any indications of strong interactions of compound **3** with the underlying NaCl surface.

Figure 3f shows an AFM image of compounds **1** and **3** in vicinity of each other. It is not surprising that these molecules appear quite different in AFM images. For example, the differences in brightness of the two molecules in Fig. 3f result from a different adsorption height[40], which was about 0.2 Å smaller for aryne than for DINP. However, the question arises whether the final product corresponds to aryne. To this end, we also performed AFM imaging of closely related NP molecules (**4**) for comparison with an aryne. AFM images of individual aryne and NP molecules are presented in Figs. 4a and 4b, respectively. The most striking differences arise for the on-axis rings at the aryne-related end and the adjacent ring. The end is characteristically curved for arynes, whereas for NP sharp kinks at the apparent carbon positions are visible. Moreover, additional features are resolved at the positions of C-H bonds and can best be seen in the Laplace-filtered images in Figs. 4d and 4e. The adjacent ring appears larger for NP than for aryne.

Beyond that, a closer look reveals more subtle differences referring to the different Kekulé depictions of arynes. The relative contributions of the resonance structures of arynes are unclear, ever since their first demonstration[41]. We thoroughly investigated the data in Figs. 4a-f in terms of differences in bond orders[34] using the empirical scheme proposed by Pauling[42] as a qualitative and easy-to-obtain quantity[43]. The Pauling bond orders for structures **3a-c** and **4** are depicted in Figs. 4g-i (greater bond orders correspond to shorter

bonds). Note that the bond orders of NP (**4**) are identical to the biradical representation (**3c**, Fig. 4i) of aryne. In our analysis, we will discuss in particular the bonds highlighted in Fig. 4d and 4e. The bonds in the central part of the molecule, highlighted in orange, are ideally suited for a bond-order analysis[34]. In the case of NP, the bond orders are 0.17 for the bond perpendicular to the symmetry axis, and 0.3 for the two adjacent ones. In agreement with that, the former bond is measured clearly longer than the latter ones in our data for NP (Fig. 4e). It is expected that alkyne (**3b**) contributions should lead to even more pronounced differences. On the contrary, the relative difference is much less pronounced in the case of aryne (Fig. 4d), indicating strong contributions from the cumulene resonance structure (**3a**). This observation is also in good agreement with the appearance of the three outermost bonds highlighted in green. In aryne these bonds appear very similar as expected for the cumulene (**3a**) representation, which shows identical bond orders for these three bonds. The biradical (**3c**) would be expected to show a clearly longer outermost C-C bond, as observed for NP. Finally, the triple bond of the alkyne (**3b**) would be expected to appear brighter than aromatic bonds and elongated perpendicular to the bond direction[28,29,44].

Additionally, we performed complimentary DFT calculations (see Methods and Supplementary Information) of free aryne and NP molecules. The resolution of the simulated AFM images based on the calculated molecules is too low (due to the high computational cost of the calculations) to resolve the subtle differences in the inner part observed in the experiment. However, the outer parts, for which the distortions are highest, are reproduced very well by the simulated AFM images and the theory reveals how the apparent atom positions are related to the real positions of the atoms. Due to the tilting of the CO tip[34,37–39,44] all the atoms and bonds at the periphery of the molecule appear displaced towards the outside of the molecule. The displacement of the outermost bond on the symmetry axis is more pronounced for the aryne than for the NP molecule (Figs. 4a-f) resulting in an enlargement of the outer ring of aryne in agreement with the experiment. The length of the outermost carbon-carbon bond is calculated to be 1.26 Å for aryne. This is between a double bond and a triple bond, which have been calculated to be 1.33 Å and 1.21 Å for ethylene (ethene) and acetylene (ethyne) molecules, respectively. We conclude from our AFM data that the cumulene (**3a**) resonance structure plays the dominant role for this aryne. The remaining contributions are rather from the alkyne (**3b**) than from the biradical (**3c**) representation, as suggested by DFT calculations.

The stability observed for aryne molecules during imaging with different tip terminations (Cu, CO, and I) may raise doubts regarding their chemical reactivity, and thus, their arynic nature. To this end, we have investigated two possible on-surface reaction schemes. First, we discuss the situation depicted in Fig. 5a, in which the I atoms are lying close to the aryne molecule. After a manipulation event (as discussed above), the atoms are at positions close to those of bonded atoms of DINP (Fig. 5b, in contrast to Figs. 2e and Fig. 3b). Finally, Fig. 5c shows that a subsequent manipulation event has initiated bond formation and thereby regenerated DINP. Note that this regeneration of DINP was only observed if both I atoms were positioned in close vicinity to the bonded positions of DINP. Orbital imaging performed before and after the dissociation-and-healing process unambiguously proves that the molecule is indeed an intact DINP (see Supplementary Fig. S1). This data provides a strong evidence that the activity of aryne is preserved on the surface. It should be mentioned that the diiodination of arynes is a known chemical transformation in solution chemistry[45]. In fact, this reaction was used to prepare a key building block within this work (see section 3.3 in the Supplementary Information, synthesis of triflate **12**).

In a different experiment, we performed dehalogenation of DINP molecules adsorbed on the bare Cu(111) surface (see Fig. 5d). The result of a voltage pulse at $V \approx 2\,\mathrm{V}$ is shown in Fig. 5e. On the bare Cu surface, the I atoms result in a much weaker contrast than on NaCl suggesting covalent bonding to the metal resulting in a lower adsorption height; but more importantly, the resulting molecular structure is very different, namely, only two out of three on-axis aromatic rings can readily be resolved. However, adjusted constant-height AFM images[40], presented in Fig. 5f, reveal that the outermost ring is in fact present, but bent towards the surface, that is, the aryne immediately forms strong covalent bonds to the Cu surface, in agreement with previous studies on dehydrogenated phthalocyanine molecules[23] and benzyne adsorbed on other metal surfaces[32,46].

In summary, we have presented direct imaging of the chemical structure of individual arynes for the first time. Our experiments provide deep insight into a class of transient species that, in general, remain obscured because of their short lifetimes. The fact that the arynes' chemical reactivity is preserved even at cryogenic temperatures is promising for novel on-surface reaction schemes, for example, for the preparation of graphene-based materials, and in order to get insight into new aryne transformations. In general, the approach presented here might also be applicable for other short-lived reaction intermediates. Furthermore,

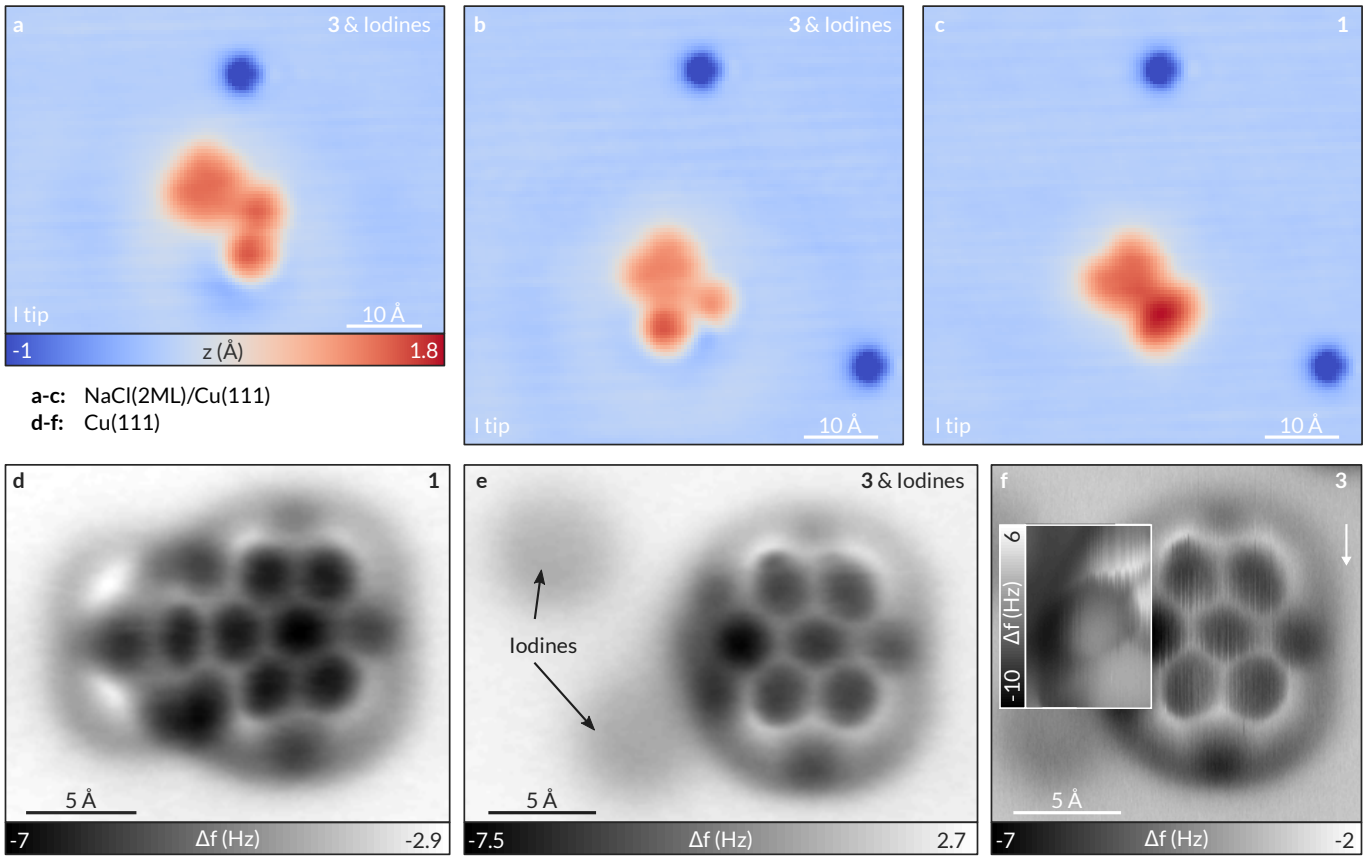

Figure 5: On-surface chemistry of an aryne. a-c, Sequence of STM images ($V = 0.2\,\mathrm{V}$, $I = 2\,\mathrm{pA}$) on NaCl(2ML)/Cu(111) proves reversibility of dehalogenation. A voltage pulse after scan **b** results in an intact DINP molecule. **d,e,** AFM images before ($\Delta z = 1.3\,\text{Å}$) and after ($\Delta z = 1.2\,\text{Å}$) dehalogenation of DINP on Cu(111), respectively. **f**, Adjusted constant-height AFM image of the same molecule with $\Delta z = 2.7\,\text{Å}$ in the highlighted region and $\Delta z = 1.3\,\text{Å}$ elsewhere. An adjusted grey scale is used for this region, as indicated. The white arrow indicates the fast scan direction (in all other data shown, it is horizontal).

we have shown that even extremely small changes, like two missing hydrogen atoms in the chemical structure, can be resolved with AFM imaging. Analysis of bond-order-related contrast showed significant differences for the molecules investigated and indicated the dominant contribution of the cumulene representation for the aryne generated under these conditions. This new kind of chemical sensitivity[47] underlines the potential of chemical structure identification by means of non-contact AFM.

Methods

Synthesis

Details on the synthesis and spectroscopic characterization of all compounds and necessary precursors are given in the Supplementary Information.

Sample preparation

Ultra-thin NaCl films were grown by thermal evaporation of NaCl on Cu(111) single crystals at a sample temperature of about 270 K. Defect-free, (100)-terminated islands of mainly two atomic layers were formed. Cu single crystals were cleaned by several sputtering and annealing cycles.

Low coverages of DINP (**1**), NP (**4**), and CO molecules were adsorbed at sample temperatures below 10 K.

STM/AFM experiments

Measurements were performed using a home-built combined STM and AFM operating in ultrahigh vacuum (base pressure below 10^{-10} mbar) at a temperature of 5 K. The voltage V was applied to the sample. The AFM is based on a qPlus sensor[48] operated in frequency-modulation mode[49]. All AFM images were acquired at $V = 0$ V with an oscillation amplitude of 0.5 Å. Positive constant-height offsets Δz correspond to a distance decrease with respect to an STM set point current of $I = 2$ pA at $V = 0.2$ V above the clean NaCl(2ML)/Cu(111) or Cu(111) surfaces, respectively.

Cu and CO tips were prepared and functionalised as described elsewhere[30,50]. I tips can be prepared in a similar manner.

Simulated AFM images

The geometries of aryne and NP molecules were calculated with density functional theory (DFT). Details of the calculations are given in the Supplementary Information.

References

1. Stoermer, R. & Kahlert, B. Über das 1- und 2-Brom-cumaron. *Ber. Dtsch. Chem. Ges.* **35,** 1633–1640 (1902).
2. Wenk, H. H., Winkler, M. & Sander, W. One century of aryne chemistry. *Angew. Chem., Int. Ed.* **42,** 502–528 (2003).
3. Roberts, J. D., Simmons, H. E., Carlsmith, L. A. & Vaughan, C. W. Rearrangement in the reaction of chlorobenzene-1-^{14}C with potassium amide. *J. Am. Chem. Soc.* **75,** 3290–3291 (1953).
4. Kitamura, T. Synthetic methods for the generation and preparative application of benzyne. *Aust. J. Chem.* **63,** 987–1001 (2010).
5. Hoffmann, R. *Dehydrobenzene and cycloalkynes* (Academic Press, New York and London, 1967).
6. Pellissier, H. & Santelli, M. The use of arynes in organic synthesis. *Tetrahedron* **59,** 701–730 (2003).
7. Tadross, P. M. & Stoltz, B. M. A comprehensive history of arynes in natural product total synthesis. *Chem. Rev.* **112,** 3550–3577 (2012).
8. Pérez, D., Peña, D. & Guitián, E. Aryne cycloaddition reactions in the synthesis of large polycyclic aromatic compounds. *Eur. J. Org. Chem.* **2013,** 5981–6013 (2013).
9. Xiao, J. *et al.* Synthesis and structure characterization of a stable nonatwistacene. *Angew. Chem., Int. Ed.* **51,** 6094–6098 (2012).

10. Schuler, B. *et al.* From perylene to a 22-ring aromatic hydrocarbon in one-pot. *Angew. Chem., Int. Ed.* **53,** 9004–9006 (2014).

11. Goetz, A. & Garg, N. Regioselective reactions of 3,4-pyridynes enabled by the aryne distortion model. *Nat. Chem.* **5,** 54–60 (2012).

12. Zhong, X. *et al.* Aryne cycloaddition: Highly efficient chemical modification of graphene. *Chem. Commun.* **46,** 7340–7342 (2010).

13. Criado, A. *et al.* Efficient cycloaddition of arynes to carbon nanotubes under microwave irradiation. *Carbon* **63,** 140–148 (2013).

14. Hoye, T. R., Baire, B., Niu, D., Willoughby, P. H. & Woods, B. P. The hexadehydro-Diels–Alder reaction. *Nature* **490,** 208–212 (2012).

15. Hoffmann, R. W. & Suzuki, K. A "hot, energized" benzyne. *Angew. Chem., Int. Ed.* **52,** 2655–2656 (2013).

16. Niu, D., Willoughby, P. H., Woods, B. P., Baire, B. & Hoye, T. R. Alkane desaturation by concerted double hydrogen atom transfer to benzyne. *Nature* **501,** 531–534 (2013).

17. Niu, D. & Hoye, T. The aromatic ene reaction. *Nat. Chem.* **6,** 34–40 (2014).

18. Godfrey, P. D. Microwave spectroscopy of benzyne. *Aust. J. Chem.* **63,** 1061–1065 (2010).

19. Radziszewski, J. G., Hess, B. A. & Zahradnik, R. Infrared spectrum of *o*-benzyne: experiment and theory. *J. Am. Chem. Soc.* **114,** 52–57 (1992).

20. Warmuth, R. o-benzyne: Strained alkyne or cumulene? NMR characterization in a molecular container. *Angew. Chem., Int. Ed.* **36,** 1347–1350 (1997).

21. Jiao, H., Schleyer, P. v. R., Warmuth, R., Houk, K. N. & Beno, B. R. Theoretical studies of the structure, aromaticity, and magnetic properties of o-benzyne. *Angew. Chem., Int. Ed.* **36,** 2761–2764 (1997).

22. Hla, S.-W., Bartels, L., Meyer, G. & Rieder, K.-H. Inducing all steps of a chemical reaction with the scanning tunneling microscope tip: Towards single molecule engineering. *Phys. Rev. Lett.* **85,** 2777–2780 (2000).

23. Zhao, A. *et al.* Controlling the Kondo effect of an adsorbed magnetic ion through its chemical bonding. *Science* **309,** 1542–1544 (2005).

24. Repp, J., Meyer, G., Paavilainen, S., Olsson, F. E. & Persson, M. Imaging bond formation between a gold atom and pentacene on an insulating surface. *Science* **312,** 1196–1199 (2006).

25. Gross, L., Mohn, F., Moll, N., Liljeroth, P. & Meyer, G. The chemical structure of a molecule resolved by atomic force microscopy. *Science* **325,** 1110–1114 (2009).

26. Mohn, F. *et al.* Reversible bond formation in a gold-atom-organic-molecule complex as a molecular switch. *Phys. Rev. Lett.* **105,** 266102 (2010).

27. Zhang, J. *et al.* Real-space identification of intermolecular bonding with atomic force microscopy. *Science* **342,** 611–614 (2013).

28. De Oteyza, D. G. *et al.* Direct imaging of covalent bond structure in single-molecule chemical reactions. *Science* **340,** 1434–1437 (2013).

29. Riss, A. *et al.* Local electronic and chemical structure of oligo-acetylene derivatives formed through radical cyclizations at a surface. *Nano Lett.* **14,** 2251–2255 (2014).

30. Mohn, F., Schuler, B., Gross, L. & Meyer, G. Different tips for high-resolution atomic force microscopy and scanning tunneling microscopy of single molecules. *Appl. Phys. Lett.* **102,** 073109 (2013).

31. Dienel, T. *et al.* Dehalogenation and coupling of a polycyclic hydrocarbon on an atomically thin insulator. *ACS Nano* **8,** 6571–6579 (2014).

32. Huang, K., Leung, L., Lim, T., Ning, Z. & Polanyi, J. C. Vibrational excitation induces double reaction. *ACS Nano* **8,** 12468–12475 (2014).

33. Chiang, C.-l., Xu, C., Han, Z. & Ho, W. Real-space imaging of molecular structure and chemical bonding by single-molecule inelastic tunneling probe. *Science* **344,** 885–888 (2014).

34. Gross, L. *et al.* Bond-order discrimination by atomic force microscopy. *Science* **337,** 1326–1329 (2012).

35. Qiu, X. H., Nazin, G. V. & Ho, W. Vibronic states in single molecule electron transport. *Phys. Rev. Lett.* **92,** 206102–206102 (2004).

36. Sweetman, A. M. *et al.* Mapping the force field of a hydrogen-bonded assembly. *Nat. Commun.* **5,** 3931 (2014).

37. Hämäläinen, S. K. *et al.* Intermolecular contrast in atomic force microscopy images without intermolecular bonds. *Phys. Rev. Lett.* **113,** 186102 (18 2014).

38. Pavliček, N. *et al.* Atomic force microscopy reveals bistable configurations of dibenzo[a,h]thianthrene and their interconversion pathway. *Phys. Rev. Lett.* **108,** 086101 (2012).

39. Hapala, P. *et al.* Mechanism of high-resolution STM/AFM imaging with functionalized tips. *Phys. Rev. B* **90,** 085421 (2014).

40. Schuler, B. *et al.* Adsorption geometry determination of single molecules by atomic force microscopy. *Phys. Rev. Lett.* **111,** 106103 (2013).

41. Laing, J. W. & Berry, R. S. Normal coordinates, structure, and bonding of benzyne. *J. Am. Chem. Soc.* **98,** 660–664 (1976).

42. Pauling, L., Brockway, L. O. & Beach, J. Y. The dependence of interatomic distance on single bond-double bond resonance. *J. Am. Chem. Soc.* **57,** 2705–2709 (1935).

43. Sedlar, J., Anđelić, I., Gutman, I., Vukičević, D. & Graovac, A. Vindicating the Pauling-bond-order concept. *Chem. Phys. Lett.* **427,** 418 (2006).

44. Moll, N. *et al.* Image distortions of a partially fluorinated hydrocarbon molecule in atomic force microscopy with carbon monoxide terminated tips. *Nano Lett.* **14,** 6127–6131 (2014).

45. Rodríguez-Lojo, D., Cobas, A., Peña, D., Pérez, D. & Guitián, E. Aryne insertion into I–I σ-bonds. *Org. Lett.* **14,** 1363–1365 (2012).

46. Johnson, K., Sauerhammer, B., Titmuss, S. & King, D. A. Benzene adsorption on Ir(100) studied by low-energy electron diffraction I–V analysis: Evidence for formation of tilted benzyne. *J. Chem. Phys.* **114,** 9539–9548 (2001).

47. Sugimoto, Y. *et al.* Chemical identification of individual surface atoms by atomic force microscopy. *Nature* **446,** 64–67 (2007).

48. Giessibl, F. J. Atomic resolution on Si(111)-(7x7) by noncontact atomic force microscopy with a force sensor based on a quartz tuning fork. *Appl. Phys. Lett.* **76,** 1470–1472 (2000).

49. Albrecht, T. R., Grütter, P., Horne, D. & Rugar, D. Frequency modulation detection using high-Q cantilevers for enhanced force microscope sensitivity. *J. Appl. Phys.* **69,** 668–673 (1991).

50. Gross, L. *et al.* Investigating atomic contrast in atomic force microscopy and Kelvin probe force microscopy on ionic systems using functionalized tips. *Phys. Rev. B* **90,** 155455 (2014).

Acknowledgments

We thank R. Allenspach for valuable comments on the manuscript. The research leading to these results has received funding from the EU projects PAMS (agreement no. 610446), the ITN QTea (317485), the ERC Advanced Grant CEMAS (291194), and from the Spanish Ministry of Science and Competitiveness (MINECO, MAT2013-46593-C6-6-P, CTQ2013-44142-P) and FEDER.

Contributions

N. P., B. S., G. M. and L. G. performed the STM/AFM experiments. S. C., Do. P., E. G. and Di. P. synthesized the molecules. N. M. performed the DFT calculations. All authors discussed the results and contributed to the manuscript.

Corresponding authors

Correspondence and requests for materials should be addressed to N. P. (pav@zurich.ibm.com) or Di. P. (diego.pena@usc.es).

Competing financial interests

The authors declare no competing financial interests.